Linear Spectroscopic Studies of Semiconductor Quantum Wells

by

M. W. Day

A thesis submitted to the

Faculty of the University of Colorado in partial fulfillment

of the requirements for Honors' designation for the degree of

Bachelor of Science

Department of Physics

2015

This thesis entitled:
Linear Spectroscopic Studies of Semiconductor Quantum Wells
written by M. W. Day
has been approved for the Department of Physics

_____

Prof. Steven Cundiff

_____

Prof. James Thompson

_____

Prof. Judith Packer

Date _____

The final copy of this thesis has been examined by the signatories, and we find that both the content and the form meet acceptable presentation standards of scholarly work in the above mentioned discipline.

Day, M. W. (B.S.)

Linear Spectroscopic Studies of Semiconductor Quantum Wells

Thesis directed by Prof. Steven Cundiff

Manufacturing processes unintentionally introduce fluctuations in the width of semiconductor quantum wells. These fluctuations subtly modulate the optical emission energies of exitons confined within the quantum well layer. It is therefore imperative to quantify these width fluctuations so their effect on exiton confinement potentials can be accounted for in ultrafast spectroscopic studies of semiconductor quantum wells. The use of microphotoluminescence spectroscopy makes quantifying this disorder possible. I present microphotoluminesence spectroscopy work taken in pursuit of an Honors' thesis.

Dedication

Long Dedication

Acknowledgements

Long Ack

Contents

Chapter

Tables

Table

Figures

Figure

Chapter 1

Introduction

Semiconductor nanostructures provide uniquely manipulable platforms for probing quantum interactions between light and matter in a highly controllable environment. These structures typically require the ability to manipulate semiconductor growth on the nanometer scale. As a consequence, manufacturing such materials is a complex and involved process. One might expect that describing electron physics within semiconductors would be an intractable problem. Indeed, exactly solving for the motion of a single electron within a crystal would be computationally impossible, as it would require solving a system of $10^2 3$ coupled differential equations. However, the Pauli exclusion principle allows for an easy way out of this problem. Because each electron in a material must occupy a different eigenstate than every other electron within that material, we can treat the behavior of electrons within crystalline lattices as a one particle problem [CITE davies].

Band theory, broadly construed, is the solution to this one particle problem. As this introduction is not meant to be a rigorous description of condensed matter physics, a brief sketch of band theory will be sufficient to explain the importance of semiconductor nanostructures. When a large number of atoms coalesce, the discrete electron states of smear into "bands" of allowed states in the atomic superstructure. In this limit, two distinct energy bands form: the valence band (lower electron energies) and the conduction band (higher electron energies). The difference between these two energies in a material is known as its "bandgap". In semiconductors, the bandgap is ten times smaller than that of an insulator

[CITE either Griffiths or Fox]. Indeed, the bandgap of many semiconductor materials is in the visible range, and thus one can photo-excite an electron from the valence band to the conduction band.

The ability to optically access a variety of states fact makes semiconductor materials ideal building blocks for optical devices. For instance, when one confines an electron in a semiconductor, the states which that electron can occupy in the conduction band of the confined material become quantized CITE Davies. Therefore, low-dimensional semiconductors make an ideal testbed for linear and nonlinear spectroscopy studies of electron dynamics in solids.

Semiconductor nanostructures are often the preferred platform for these investigations. Nanoscale manipulation of material properties allows for the manufacture of a wide array of semiconductor devices. In such devices, the confinement dimensionality (generally one, but sometimes two or three), width, and energetic depth are all free parameters. Because of this parametric freedom, everything from simple confinement schemes to complicated structural configurations have proven to be very useful for creating electronic and optoelectronic devices CITE NAT REVIEW. In addition, semiconductor nanostructures form the basis for photonic quantum information devices CITE DEVICE REVIEW, QI REVIEW.

For our purposes, we will be discussing semiconductor quantum wells (QWs). These nanostructures are layers of relatively low bandgap material (GaAs in our case) sandwiched between layers of higher bandgap ($AlGaAs_{subscriptsrelevantfordistinguishingbetweensamples,Ithink}$). If one excites an electron wto the conduction band of a material, the electron can be weakly bound to the vacancy (or "hole") it left in its parent atom. This bound electron-hole pair is known as an excition, and its importance will be elaborated on later. If an exciton is created within the QW, it can be treated theoretically using a simple particle-in-a-box quantum mechanical picture. For our purposes, QWs are extremely useful for studying the subtleties of light's interaction with matter.

Despite immense progress in the growth of quantum wells, manufacturing processes still

unintentionally introduce inhomogeneities to the layer thickness during crystal deposition. This translates to an uneven interface between two different materials on the scale of a few crystal monolayers. What this means for a quantum well structure is that small fluctuations in interface flatness translate to small fluctuations in well width as these happen at both interfaces of the quantum well and barrier layers. These small width fluctuations are known as structural disorder.

Semiconductor quantum wells are studied optically by our lab. In most of our experiments involving these structures, excitons are generated in the wells, and their dynamic behavior can be monitored by several different spectroscopic techniques, notably various linear spectroscopic methods and multidimensional Coherent Spectroscopy (MDCS). As will be shown later, small changes in well width cause changes in confinement potentials for excitons and thus affect the energies at which exciton states exist in the wells. Therefore, disorder is the main cause of inhomogeneous broadening within QW samples. This is known to be true (CITE BRISTOW), but quantifying the spatial distribution of disorder is important because complete information concerning inhomogeneous contributions to the overall spectral response of QWs can help us enrich our understanding of many-body physics of excitons within quantum wells. In this thesis, I present my development of micro-photoluminescence spectroscopy (μPL), a type of linear spectroscopy, to obtain a spatial map of emission energy fluctuations. Furthermore, I translate this spatial picture into a quantitative measurement of disorder on three different types of QW structures: a periodic ten-quantum well structure, a periodic four-quantum well structure, and an interfacial quantum dot ensemble.

In addition to studying quantum well disorder, linear spectroscopy is useful for characterizing the energy profile of electron states in matter. For example, it is useful to study exciton states the asymmetric double quantum well, as these systems are great testbeds for various quantum coupling phenomena CITE AQW Review. Understanding incoherent coupling between exciton states in asymmetric double quantum wells allows us to fulfill two important experimental goals: we obtain a better understanding of the exact absorption

energies of the various exciton states, and we can explore incoherent coupling between states in each of the wells. In addition to μ-PL experiments, I present the development of Photoluminescence Excitation Spectroscopy (PLE) to study the linear properties of exciton states within AQWs.

The thesis is structured such that Chapter 2 is a theoretical introduction to the physical concepts necessary to understand our μ-PL and PLE experiments. Chapter 3 will be a description of our experimental methods, while results of our experiments will be presented in Chapter 4. Chapter 5 will conclude this thesis with our experimental interpretations and a discussion of possible experimental directions for the future.

Chapter 2

Theory and Background

In this chapter, I will provide the theoretical background necessary to understand the work presented in this thesis. The first section will deal with the definition and importance of the bandgap of a material, the second will introduce the effects of confinement on electrons within semiconductors, leading to a discussion of experimental confinement within the semiconductor quantum well. The third section will introduce the concept of semiconductor quantum well disorder, and the fourth will motivate the study of semiconductor quantum well disorder with micro photoluminescence spectroscopy. Finally, I will discuss the optical properties of asymetric double quantum wells and how to use photoluminescence excitation spectroscopy to investigate incoherent coupling between excitons in the asymmetric double quantum wells.

2.1 The Semiconductor Quantum Well

This section will broadly lay out band theory of electron states in solids. I will then discuss interband absorption by electrons in direct-gap semiconductors.

2.1.1 Bandgap

In order to understand how electrons behave in a crystalline solid, one must first understand how bound electrons act when arbitrarily many atoms are brought together in a lattice structure. Consider a collection of N atoms sufficiently far apart such that interactions

between atoms can be neglected. In this limit, electrons in an atom such as Hydrogen occupy *discreet* energy levels. For instance: suppose all N of our atoms are monatomic hydrogen atoms. In our system, an electron behaves according to the following Hamiltonian:

$$\hat{H} = -\frac{\hbar^2}{2m} \bigtriangledown^2 - \frac{e^2}{2\pi\epsilon_0 r}. \tag{2.1}$$

We can find the electron wavefunctions $\psi(x)$ by solving the time independent Shrödinger equation,

$$\hat{H}\psi(x) = E_n\psi(x) \tag{2.2}$$

where E_n is the energy of the n^{th} energy level. This equation can be solved using the usual methods CITE Griffiths, but doing so here would be a diversion, so I'll just skip to the crucial points: evidently, the $n = 2$ electron wavefunction (again neglecting interactions between atoms and ground state perturbations) is

$$\psi(x) = Y_l^m \frac{1}{\sqrt{2}} a_0^{-3/2} \Big(1 - \frac{r}{2a_0}\Big) exp\big(-r/2a_0\big) \tag{2.3}$$

where a_0 is the Bohr radius, Y_l^m is either the $l = 0, m = 0$, the $l = 1, m = 1$, or the $l = 1, m = 1$ spherical harmonic. Note: each $n = 2$ energy level in this system is N-fold degenerate, as there are N orbitals with the same energy. Considering just the $n = 2$ states and neglecting perturbations, electrons in these states evidently all have energy

$$E_2 = \frac{-13.6eV}{n^2} = \frac{-13.6eV}{4}. \tag{2.4}$$

In the limit that many atoms are brought together such that interactions can no longer be neglected, two things happen: each N-fold degenerate electron energy level will split into N components, and these levels will become so close that they will smear into allowed and disallowed energy densities of state CITE Indonesi, Siradesh, Grif, Davies. Roughly speaking, the occupied states are known as the "valance band" states, and the unoccupied states are known as the "conduction band states". The energy difference between the valance band and conduction band is called the bandgap, and its importance will be illuminated momentarily.

These band states are simultaneous eigenstates of both the Hamiltonian and the crystal momentum CITE Davies(?). This means that bands can be easily depicted in k-space using dispersion curves. Dispersion curves map out allowed band energies in k-space, and their full functional shape is dependent on the types and arrangement of constituent atoms. Solids can be broadly organized into three categories based upon the k-space arrangement of their electron bands. In metals, the conduction band energies are below the highest energy valence band states and thus some conduction band states are occupied. In insulators, the bandgap is relatively large (about 10eV) CITE Mark Fox. By contrast in semiconductors, the bandgap is roughly 1eV and can therefore be optically accessed. Sometimes, as in the case of GaAs crystals, a local valance band minima and conduction band maxima occur for the same value of k in k-space. Semiconductors with this sort of bandstructure are known as direct-gap semiconductors. Around this value of k, electrons can absorb a photon with enough energy to undergo a direct transition from the valance band to the conduction band CITE Iandonesi, Galan thesis. This fact forms the basis of linear and nonlinear optical studies of semiconductor nanostructures (CITE Steve review), photonic devices, and certain types of theoretical quantum information processing schemes (CITE Nature Review of QI).

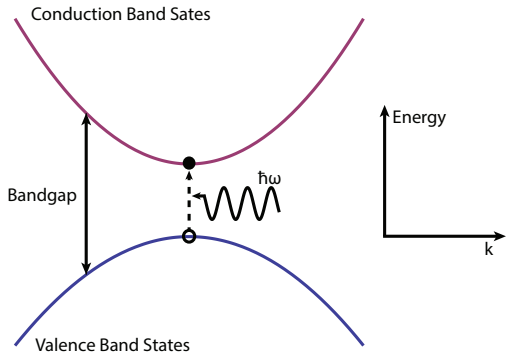

Figure 2.1: A typical dispersion curve minima for a direct-gap semiconductor. An optical transition is illustrated at $k = 0$, where an electron is absorbing a photon resulting in a transition from the conduction band to the valance band.

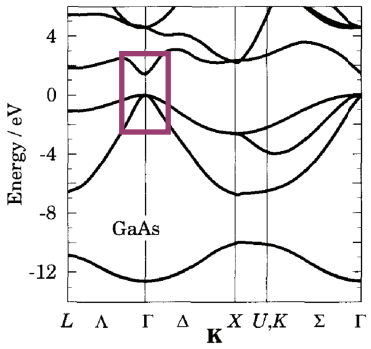

Figure 2.2: The band structure of GaAs, the allowed states are the thick horizontal curves, and the boxed region is the direct-gap region, in which electrons can be make direct transitions across the bandgap. Note, the minima of this region look like the dispersion curve in figure 2.1 CITE Davies.

2.1.2 Confinement

It is well known that nanometer scale confinement of particles results in quantized energy states CITE Griffiths. In the previous section, I briefly introduced the bandgap, and its important physical properties. In this section, I'll illustrate an interesting application of band theory: the semiconductor quantum well (QW). First, it is important to understand what we mean by confinement, and how quantized energy levels arise for confined particles. I will draw an analogy to a familiar physical situation, the particle confined within an infinite potential. I will then use this analogy to construct a physical picture for QWs, and then I will discuss the formation of excitons and a simple physical model of their behavior, sufficient for understanding the spectroscopy conducted in this thesis.

Perhaps the simplest problem in quantum mechanics is the of confinement of a particle in an infinite, one dimensional potential well. I will sketch a derivation of the wave function of a particle trapped in such a well, and use this derivation as the basis for exploring the physics of the QW exciton. We will begin by considering an arbitrary particle confined in a one dimensional infinite potential well. The potential that our arbitrary particle feels is:

$$V(x) = \begin{cases} 0 & 0 < x < L \\ \infty & |x| > 0 \end{cases}$$

where L is the length of the potential well. Graphically, the potential the particle feels looks like 2.1.2.

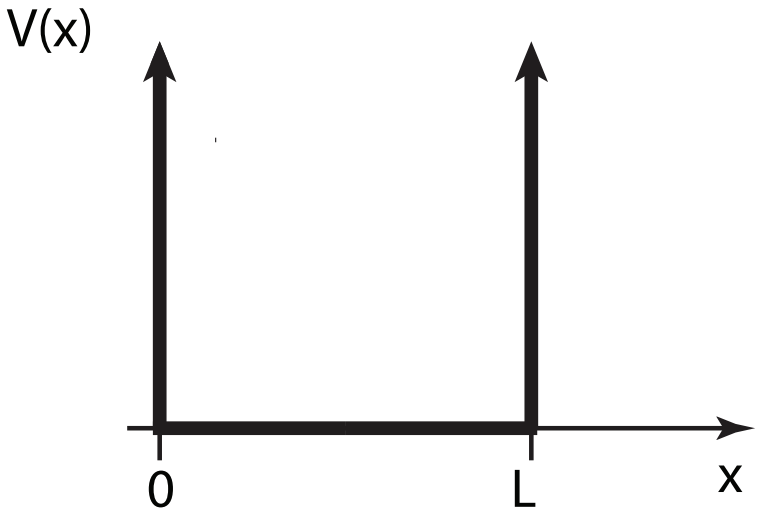

Figure 2.3: A graphical representation of the one-dimensional infinite potential well of width L.

Our task is to solve the time independent Schrödinger equation to show how quantized bound states arise for one-dimensional confinement. The time independent Schrödinger equation reads:

$$\hat{H}\psi(x) = E\psi(x) \tag{2.5}$$

where E is the energy of the particle, and $\psi(x)$ is the particle's wavefunction. The particle will evidently be confined to the well, so our Hamiltonian inside the well is just

$$\hat{H} = -\frac{\hbar^2}{2m}\frac{\partial^2}{\partial x^2} \tag{2.6}$$

where m is the particle's mass, and E is the particle's total energy. The time independent Schrödinger equation now reads:

$$\frac{\partial^2}{\partial x^2}\psi(x) = -\alpha\psi(x) \tag{2.7}$$

where we define

$$\alpha = \frac{2mE}{\hbar^2}. \tag{2.8}$$

Now, eq. 2.7 looks like the familiar simple harmonic oscillator equation from classical mechanics. Because the wave function must be continuous at $x = L$ and $x = 0$, i.e. it vanishes at those locations, and the potential is odd about the origin, solutions to eq. 2.7 have the form:

$$\psi(x) = Asin(kx) \tag{2.9}$$

where k contains E and is determined by our boundary conditions. Now we want $\psi(L)$ to vanish, but we can't have $A = 0$, because that is the trivial solution to eq. 2.7. Therefore, because we want $\psi(L) = Asin(kL) = 0$, we must have $ka = \pm n\pi$ where $n \in \mathbb{N}$. Now, we can absorb all of the negative combinations of kL into our normalization constant, A, and we have, then, that

$$k_n L = n\pi \tag{2.10}$$

where the subscript denotes the fact that we now have infinitely many, *discreet* solutions to eq. 2.5. Evidently

$$k_n = \frac{n\pi}{L} \tag{2.11}$$

and therefore

$$\psi(x) = Asin(\frac{n\pi x}{L}). \tag{2.12}$$

Now, if we let $k_n = \alpha$ and solve for E, we obtain

$$E = \frac{n^2\pi^2\hbar^2}{2mL^2}. \tag{2.13}$$

It will do us no good to normalize the wavefunctions we found, as their use for our purposes is minimal. The important part is that confinement in one dimension resulted in our particle occupying *discreet* energy levels whose energy depends on the size of the confinement potential.

Using layers of semiconductors, one can generate similar one-dimensional confinement effects for electrons. A simple way this can be done is by sandwiching a layer of low-bandgap semiconductor material in between two layers of higher bandgap materials (CITE Davies). One period of this structure is shown in figure 2.4. If the well material is a direct-gap semiconductor, then simple optical transitions (i.e. not mediated by phonons) across the bandgap can be made, as the transition illustrated in figure 2.1. Figure 2.5 is the band structure for GaAs, the chosen well material for the studies of growth disorder. Annotated on the figure is the direct-gap transition zone of interest. The potential well created by the semiconductor sandwich leads to quantization of electron states within the well layer CITE Miller, Davies, Steve Review. We can access each of these states optically, making the QW a great testbed for exploring electron dynamics within a simple and well-known potential CITE Steve Review.

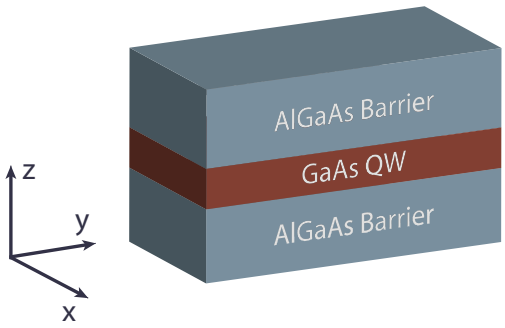

Figure 2.4: An example of the semiconductor quantum well. These layers can be repeated arbitrarily many times.

2.1.3 The Exciton

The simple picture presented above doesn't quite adequately represent the physics of an electron within a quantum well, however. After an excited electron moves from the valence band to the conduction band, it will leave behind a vacancy, or "hole", around its parent atom CITE Miller, Davies. The electron feels a *screened* Coulomb potential from this vacancy, as the vacancy is positively charged. I'll briefly sketch why this potential arises and then introduce the key concept of this section: the excition. Imagine a number of electrons have been excited within the QW. Now, spatially, one will have a quasi-neutral distribution of electrons and holes in the well layer: an electron-hole plasma. I will assume that the holes are stationary relative to the electrons in the well, and that the excitation density is relatively low. These assumptions are *a priori* unphysical, but they immensely simplify the derivation of the electric potential QW electrons feel, and preserve the important physical results.

Let's explore the local behavior of an excited electron due to a single adjacent hole in the QW. Note that in this picture, electrons everywhere in the QW feel a Coulomb attraction to the hole, but the electrons adjacent to the hole *screen* its effects from charges far away. This phenomenon, known in plasma physics as Debye shielding CITE Chen and in quantum mechanics as electron screening CITE Griffiths, modifies the pure Coulomb potential one would expect a single electron-hole pair to experience. We will assume that the electrons in the plasma obey a Maxwellian density distribution. Now, the local density of electrons around the hole is

$$n_e = n_0 \; exp\Big[\frac{e\phi}{kT}\Big] \tag{2.14}$$

where n_0 is the electron density far away, e is the electron charge, ϕ is the local electromagnetic potential, and T is the electron temperature. A complete derivation for this electron number density in an arbitrary plasma can be found in CITE Chen. This is the local electron

distribution, and we can assume $e\phi \ll kT$ because the potential an electron feels due to one hole can be considered small relative to its thermal energy. Taylor expanding to first order, we find that

$$n_e \approx n_0\Big[\frac{e\phi}{kT}\Big]. \tag{2.15}$$

Now, our local charge density is

$$\rho(r) = e\Big[\delta(r) - n_0\Big(\frac{e\phi}{kT}\Big)\Big] \tag{2.16}$$

where we've assumed that the hole has positive charge magnitude e, is infinitely small, and situated at the origin. The Poisson equation reads

$$\epsilon_0 \bigtriangledown^2 \phi(r) = -e\Big[\delta(r) + n_0\Big(\frac{e\phi}{kT}\Big)\Big]. \tag{2.17}$$

We can define a constant,

$$k^2 = \frac{n_0 e\phi}{\epsilon_0 kT} \tag{2.18}$$

and now the Poisson equation is

$$\big(\bigtriangledown^2 - k^2\big)\phi = -\frac{e\delta(r)}{\epsilon_0}. \tag{2.19}$$

This is known as the screened Poisson equation, and its solution is

$$\phi(r) = -\frac{e}{4\pi\epsilon_0 r}e^{-kr}. \tag{2.20}$$

Now, $\phi(r)$, functionally, *exactly* the correct result (albeit with a different k) had we proceeded under the Thomas-Fermi approximation, assuming only that the potential is weak and varies smoothly and slowly over a distance around the hole equivalent to $\frac{1}{k_f}$. This turns out to be a very good approximation for the local potential an electron feels relatively close to a hole CITE Patterson. The single-particle hamilltonian for an electron in the QW is now:

$$\hat{H} = -\frac{\hbar^2}{2m}\frac{\partial^2}{\partial x^2} - \frac{e}{4\pi\epsilon_0 r}e^{-k_0 r} \tag{2.21}$$

where $k_0^2 = \frac{n_0 e\phi}{kT_f}$ is the "corrected" k for the same potential derived under the Thomas-Fermi approximation CITE Patterson.

Note that if the potential electrons feel was exactly Coulombic in nature, then any bound state between an electron and a hole would be hydrogenic CITE Griffiths. This potential, however, is *not* exactly Culombic in nature, so the bound states between the electrons and holes can't be described by hydrogenic wavefunctions. Nevertheless, bound states between an exited electron and an adjacent hole do exist, and when an electron and hole occupy these states, they form a quasiparticle called an "exciton", and they can be treated as a single particle with an effective mass CITE Davies, Iandonesi, Rogers.

The subtleties of the wave function are treated in CITE Rogers, exploring their exact functional form and corresponding density of exciton states in the QW will not be of use to us here. Only energy levels of the QW exciton are discretized by its confinement, those of excitons created in the bulk are not. A final important note: in both my derivation and those proceeding under the Thomas-Fermi approximation, the hole is assumed to be a *stationary* point particle. This is emphatically *not* true, but the physics doesn't change that much if we assume both charge carriers are mobile. Excitons can still be treated as a single particle even removing this assumption. Figure 2.5 depicts a simple physical picture for excitons: the electron and hole excited energy levels can be thought of as the ground state of a particle trapped in a finite potential.

2.2 Quantum Well Disorder

When an exciton is optically created, in a direct gap semiconductor such as GaAs, the charge carriers can recombine from the either exciton "ground" state ($n = 1$), or "excited" states ($n > 1$) and emit a photon at the exciton binding energy CITE Gilleo. Since I am only interested in linear, long-timescale exciton physics, we can treat QW excitons as an approximately two-level system, only looking at ground state recombination. The emission energies for QW excitons will be dependent on well depth, a function of the barrier composition, and

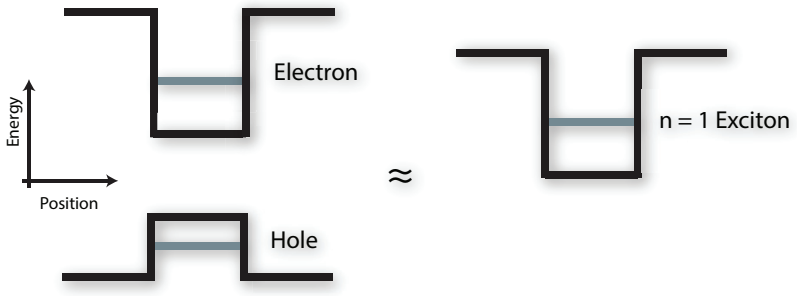

Figure 2.5: A simple model for the behavior of an exciton in a quantum well, suitable for the work completed herein.

well width. Control of QW layer thickness has improved immensely, as QW structures can be made to precise specifications with modern molecular beam epitaxial growth methods CITE Davies. However, imperfections of layer width on the order of a crystal monolayer occur unavoidably at the interface between the well and barrier materials during the QW manufacturing process CITE Yoshita Terrace paper (find better). In figure 2.6, an AFM picture of imperfections of a GaAs surface are shown. These defects, known as structural disorder, slightly change the width of the well layer and thus subtly modulate exciton emission energies, an illustration of which is shown in figure 2.7. By analogy to eq. 2.11, excitons localized in slightly thinner than average sections of the QW will emit at slightly higher energies than average. Conversely, excitons localized in thicker than average sections of the QW will emit at slightly lower energies than average. Thus, structural disorder is the main contribution to inhomogeneous broadening in the QW coherent optical response CITE Bristow.

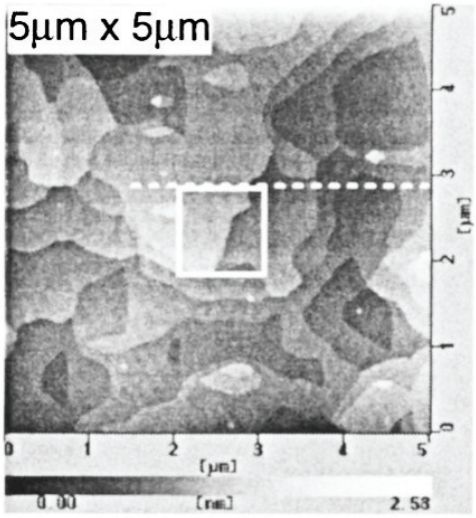

Figure 2.6: An STM picture of the GaAs growth front, stopped mid-growth, of a 110 oriented sample. The shown defect size is roughly representative of disorder in modern GaAs samples grown by molecular beam epitaxy. However, defect size and shape is highly sample dependent, so disorder varies widely from one QW structure to the next. Note, the disorder terraces are on the order of 100nm across. Taken from CITE Yoshita Terrace.

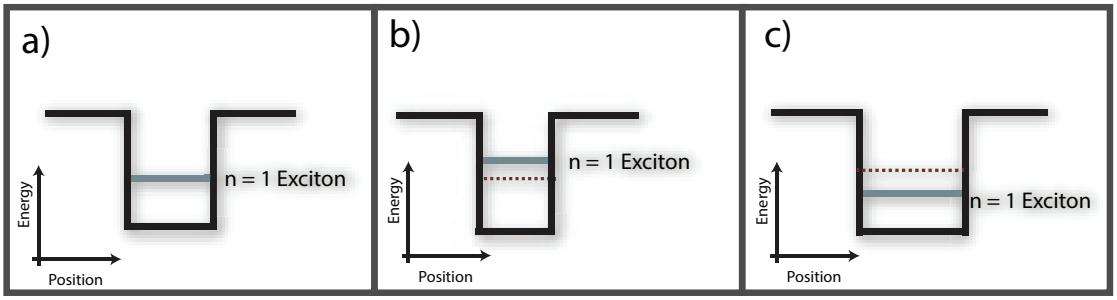

Figure 2.7: In a), the energy of a ground state exciton located in a portion of the QW of average thickness, the blue line in b) depicts the ground state energy of an exciton located in a slightly thinner than average portion of the QW, and in c), the blue line depicts the ground state energy of an exciton located in a slightly thicker than average portion of the QW. In both b) and c), the average exciton ground state energy is depicted by the maroon dashed line.

2.3 Microphotoluminescence Spectroscopy

Because local QW thickness determines exciton emission energy, a spatial picture of disorder is possible through spectral imaging. By using a continuous wave (CW) excitation source to create a population of QW excitons and monitoring the emission energy as a function of sample position, one can extract the local QW width. With sufficiently high resolution, obtaining a map of emission energies for a representative portion of a QW sample is possible. In order to obtain a map of emission energies, one must monitor the photoluminescence (PL) energies as a function of position CITE Steve's theory reccomendation. In a PL experiment, light of sufficiently high energy is shown on a sample, exciting a large number of charge carriers to the conduction band. During this process, electrons fall back into holes in the valance band, emitting a photon equivalent to the lost energy CITE Davies. If a QW exciton recombines, it will emit a photon equivalent the energy difference between the valance band and one of the quantized exciton states. If we regard the exciton as a two level system, by exciting QW excitons near-resonantly, the energy of the emitted photon will be equivalent to the energy difference between the valance band and the exciton ground state.

In order to obtain an image of PL, we must collect the signal carefully. More precisely, if we are to obtain a spatial picture of QW disorder, we must collect and spectrally resolve a PL image. The PL will be emitted from the exciton population over a 4π solid angle, so we must place the QW directly at the focus of our imaging system in order to form a clear PL image. Furthermore, since the scale of the disorder is on the order of 100nm CITE Yoshita Terrace paper, we must have comparable resolution for the PL image. Measuring a PL image is fairly easy, one must place the QW at the focus of a pair of lenses in a confocal optical geometry. Figure 2.8 is a diagram of this setup, and the magnification of the PL image is set by the ratio of the lens focal lengths. Namely,

$$M = \frac{f_1}{f_2} \tag{2.22}$$

where f_2 and f_1 are the focal lengths of the short focal length lens and the long focal length lens respectively, and M is the image magnification factor. A PL experiment with sub-micron resolution which is capable of spectrally resolving a PL image is known as a "microphotoluminescence spectroscopy" experiment, or μPL.

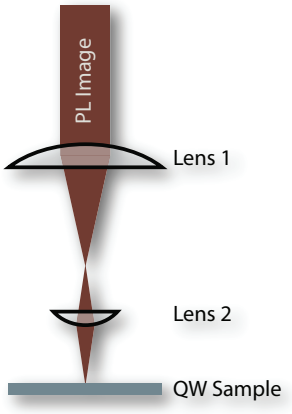

Figure 2.8: A representation of a confocal optical geometry used to collect the PL from the QW sample. The PL image is being collected from a small region of the QW sample, magnified, and then collimated by the two lenses.

As simple as the PL image collection is, it is difficult to obtain the requisite image resolution because the PL is around 750-800nm wavelength, but as I've asserted above, the islands can be smaller than this. What this means is that if we were able to image at the Abbe diffraction limit of our optical geometry, we still wouldn't have the resolution necessary to resolve adjacent disorder sites. The Abbe diffraction limit is

$$d = \frac{\lambda}{2nNA} \tag{2.23}$$

where λ is the wavelength of the PL image, n is the index of refraction in the intermediate space between the sample and lens 2 (the imaging lens) in figure 2.8, and NA is the numerical aperture of lens 2. Note that $NA = f/D$ where f is the focal length of the imaging lens and D is its diameter. In our case, $d \approx 500nm$ for $\lambda \approx 780nm$, $n = 1$ in vacuum, and we pick

$NA = .83$, as that was the NA of the lens in our experimental setup.

In order to get around this limit, we either need to resort to exotic microscopic techniques, or we can employ a fairly simple trick. It has been shown that by increasing the index of refraction (n) with a solid immersion lens (SIL), the Abbe diffraction limit can be substantially reduced CITE Yoshita Application paper, and broad SIL paper. In order to do this, one simply places a hemisphere of sufficiently high n material between the sample and the imaging lens. Figure 2.9 is a diagrammatic representation of this improvement. Note, I'll use SIL and hemisphere interchangeably from here on out, though they aren't necessarily interchangeable, as "SIL" refers to a truncated sphere of some degree.

In my experimental setup, I used a Zinc Selenide (ZnSe) SIL, for which $n = 2.4$ at $\lambda = 780nm$. This improvement decreases the diffraction limit from $d \approx 500nm$ to $d \approx 185nm$, roughly sufficient resolution for our purposes. I'll expand on the precise setup in the next chapter, but the experiment will be very similar to what I've just described.

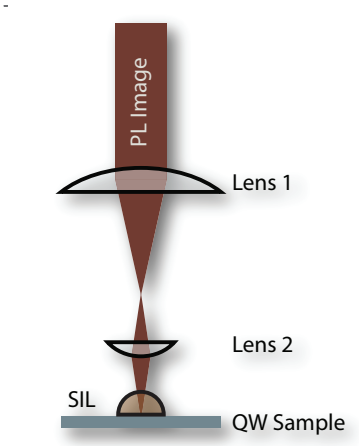

Figure 2.9: A representation of the principle of our specific μPL experiment. The PL image leaves the SIL normal to the hemispheric surface, so it just increases n and lowers the diffraction limit.

2.4 Exciton Coupling in Asymmetric Double Quantum Wells

(Summary, flesh out)

Quantum coupling between excitons occurs when multiple quantum wells get close enough so that the exciton wavefunction can tunnel slightly into other wells CITE Griff, Davies (?). In order to study quantum coupling between states in adjacent QWs, however, it is not simply enough to grow multiple quantum well layers fairly close to one another. Evidently, if each of the wells is of identical thickness, then QW PL from one well will be spectrally indistinguishable from another CITE Thomas. Indeed, it is necessary to grow wells of varying thickness when studying coupling in multiple quantum wells CITE Heagarty. In this thesis, I will only discuss incoherent coupling of exciton states in various asymmetric double quantum well (AQW) samples.

2.5 Photoluminescence Excitation Spectroscopy

(PLE Papers from my lit. review, Chris', suggestions from Steve. In lib1, Zotero)

Chapter 3

Experimental Methods

In this chapter I will describe the experiments I conducted for this thesis. The first section will deal cover the configuration and customization of the continuous wave (CW) Titanium Sapphire laser I used as an excitation source for conducting both PLE and μPL experiments. Section two will cover the design and construction of the in-cryostat optic mount for the μPL experiment as well as the optical configuration for data collection. Section three will illustrate the data collection procedure used in μPL experiments, as well as the function and implementation of LabView code I wrote for hardware control and data acquisition. In section four, I will lay out the optical design of our PLE experiments and in section five, I will discuss the experimental data collection process and signal optimization routines.

3.1 The Light Source

The PLE and μPL experiments required a CW laser light source with a few properties: the laser must be a stable and fairly high-power light source with narrow line-width. For μPL, it was important that we have a fairly Gaussian and symmetric beam so we could obtain the desired spot-size and resolution at the sample. Additionally, conducting PLE scans required that we have the ability to computer control the laser wavelength over a fairly broad range of wavelengths, roughly a spectral region from $\lambda = 780$nm to $\lambda = 850$nm. The laser we chose for this task was a Schwartz Electro Optics Titan-CW Titanium Sapphire

(Ti:Sapph) laser. Its specifications were fairly close to our needs, as its specified operating power is 500mW with a tunable range from roughly 700-820nm CITE Titan manual.

The laser cavity can be configured for either CW or pulsed operation. In CW operation a 532nm pump beam, 5W of power, enters the cavity through a series of steering mirrors. After entering, the pump passes through a lens to focus the pump on the Ti:Sapph crystal. After the gain medium, the remaining pump light passes through the end mirror and terminates at the back of the laser enclosure. The laser configuration is shown in figure 3.1.

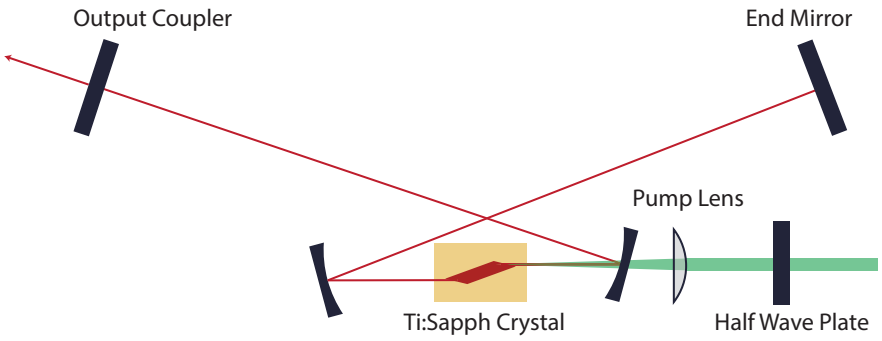

Figure 3.1: A depiction of the modified mount: the actuator arm fits into a sleeve attached by a pivot to the rotating filter mount. A spring attached to both the rotating mount and aluminum block holds the sleeve to the actuator and ensures smooth rotation in either direction.

Though the Ti:Sapph laser nearly met our specifications, it required two modifications to be operable in our experiments. First, we needed to add a computer controlled actuator to rotate the the birefringent tuner in order to allow for increased tenability and repeatability relative to a manually actuated micrometer. We modified the rotation mount for the birefringent filter (BRF) to accommodate a Newport TRB25 linear actuator. The linear actuator pushed a spring-loaded arm to rotate the BRF to a specified angle and select our desired wavelength. Figure 3.2 depicts the modified BRF mount with Newport actuator attached.

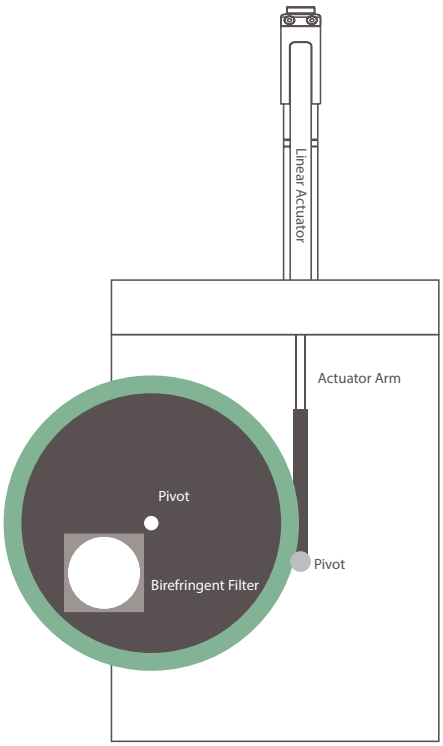

Figure 3.2: A depiction of the modified mount: the actuator arm fits into a sleeve attached by a pivot to the rotating filter mount. A spring attached to both the rotating mount and aluminum block holds the sleeve to the actuator and ensures smooth rotation in either direction.

3.2 Optical Components and Optical Path Configuration

3.2.1 Manufacturing the SIL

In order to obtain the resolution necessary to image disorder, the experiment employed a solid immersion lens (SIL) at the surface of the sample to increase the index of refraction at the imaging plane. I chose ZnSe as the SIL material, as its index of refraction at 780nm is n=2.4 CITE website. However, ZnSe SILs are not commercially available, so I resorted to manufacturing SILs from a stock ZnSe window. The window measured 2.54cm diameter by 1cm thickness, and our goal was to manufacture SILs of roughly 3mm in radius. To begin, we used a core drill, diameter 6.35mm, to cut out a cylindrical chunk of ZnSe. I then

centered and glued the cylindrical stock material to a brass dowel, 2mm in radius. After the ZnSe was glued to the rod, the SIL shaping began. I put the brass dowel in a power drill used 200 grit sandpaper to shape the ZnSe cylinder roughly into a hemisphere.

When the SIL was in the roughly correct shape, we lapped and polished the hemispherical surface until the SIL was at the correct size. Additionally, since the experiment required optical quality surfaces, this was a careful and fairly lengthy process. I made the polishing lapps by machining a 2.54cm diameter copper rod to roughly 2cm in diameter with a 1.8cm wide by 1cm deep cavity. Then, I melted lead solder into the cavity, let it harden, and machined the face of the copper and solder until they were flush and mahcine-smooth. Then, I pressed a cleaned, 6.35mm dieameter ball bearing halfway into the solder. Figure 3.3 depicts what a finished lapp looked like before it was used to grind and polish the SIL.

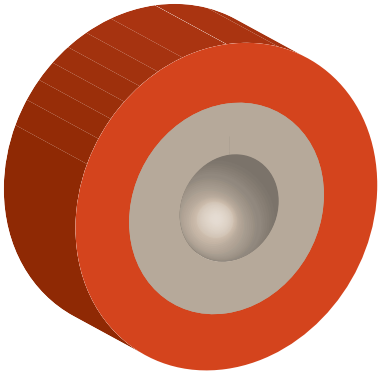

Figure 3.3: A depiction of the lapp. The orange casing is copper while the grey lining is lead solder. The cavity left by the ball bearing was smooth enough to polish the relatively soft ZnSe hemispheres.

After the lapp was made, we mounted the dowel with the SIL still attached to a glass lathe. As the lathe rotated, we placed the lapp with a mixture of glass polishing solution of various grit and mineral oil onto the SIL and held it in place with a sharpened wire. The wire and Lapp were both off center so the friction of the rotating SIL would randomly move the lapp so as to evenly polish the surface of the hemisphere. A depiction of this setup is in

figure 3.4. (GRIT SIZE INFO). After the process was finished, the SIL was removed from the dowel and the flat surface was poilshed with a colloidal silicon mixture. When the SIL was finished, we had a hemispherical (to within 1%) ZnSe SIL.

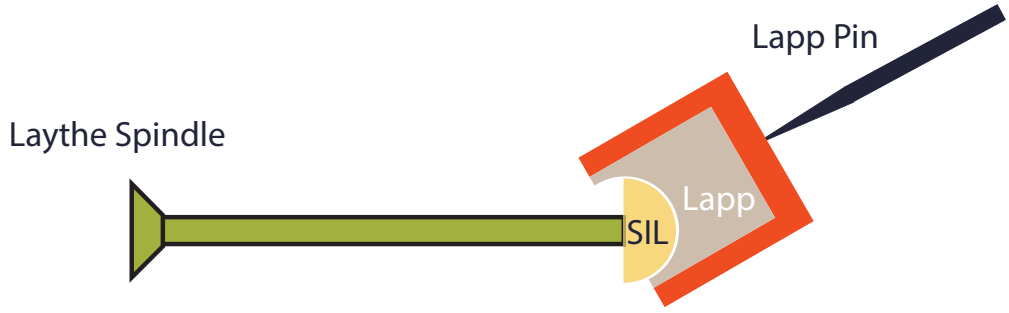

Figure 3.4: A depiction of the polishing setup in the lathe. The off-center placement of the lapp and lapp pin allowed the lapp to rotate and move slightly to randomize the SIL polishing.

3.3 Cryostat Optics